JACS
JOURNAL OF THE AMERICAN CHEMICAL SOCIETY
Communication
pubs.acs.org/JACS

Passive Tumor Targeting of Renal-Clearable Luminescent Gold Nanoparticles: Long Tumor Retention and Fast Normal Tissue Clearance

Jinbin Liu, Mengxiao Yu, Chen Zhou, Shengyang Yang, Xuhui Ning, and Jie Zheng*

Department of Chemistry, The University of Texas at Dallas, Richardson, Texas 75080, United States

Supporting Information

ABSTRACT: Glutathione-coated luminescent gold nanoparticles (GS-AuNPs) with diameters of ~2.5 nm behave like small dye molecules (IRDye 800CW) in physiological stability and renal clearance but exhibit a much longer tumor retention time and faster normal tissue clearance, indicating that the well-known enhanced permeability and retention effect, a unique strength of conventional NPs in tumor targeting, still exists in such small NPs. These merits enable the AuNPs to detect tumor more rapidly than the dye molecules without severe accumulation in reticuloendothelial system organs, making them very promising for cancer diagnosis and therapy.

Inorganic nanoparticles (NPs) with large surface areas, tunable material properties, and strong signal output[1] can potentially serve as a new generation of nanomedicines that could catalyze the shift of our current medical paradigm to "earlier detection and prevention".[2] NPs often passively accumulate in disease sites such as tumors at much higher concentrations and for longer times than small drug molecules through the well-known enhanced permeability and retention (EPR) effect,[3] making NPs even more promising in addressing many challenges that small drug molecules encounter in early cancer diagnosis and therapy.[2a] For example, 30 nm gold nanocages coated with poly(ethylene glycol) (PEG) can passively target tumors with a high efficiency of 8% injected dose per gram of tissue (% ID/g) 24 h post injection (p.i.).[4] This unique strength of NPs in tumor targeting is fundamentally due to the ability of NPs to escape kidney filtration and be retained in the blood plasma for longer times than small molecules.[3b] However, unlike small, renal-clearable, clinically used molecular probes such as 2-deoxy-2-[^{18}F]fluoro-D-glucose,[5] Gd-DTPA,[6] and iomeprol,[7] inorganic NPs often severely accumulate in reticuloendothelial system (RES) organs (liver, spleen, etc.),[8] resulting in low targeting specificity (defined as the amount of probe in tumor vs that in liver)[9] and potential long-term toxicity,[10] hampering their clinical use.

To minimize nonspecific accumulation in RES organs and potential toxicity of inorganic NPs, several different kinds of renal-clearable inorganic NPs have recently been developed.[11] For instance, Choi and co-workers[12] found that cysteine-coated CdSe/ZnS quantum dots (QDs) with hydrodynamic diameters (HDs) below 5.5 nm can be efficiently cleared into the urine within 4 h, with <10% ID of the QDs accumulated in the RES organs. Our recent studies[13] showed that glutathione (GSH) can serve as an effective surface ligand to minimize nonspecific RES uptake of few-nanometer luminescent gold NPs (GS-AuNPs), enabling >60% ID of the NPs to be cleared through the urinary system with an NP loading of only 3% ID/g found in the liver 48 h p.i.[13c] More detailed pharmacokinetics studies[13b] revealed that GS-AuNPs are rapidly distributed in the body with a short distribution half-life of 5.0 min and circulate in the body with a long blood-elimination half-life of 12.7 h in balb/c mice.

While these renal-clearable inorganic NPs behave like small molecules in urinary elimination and two-compartment pharmacokinetics because of their small size and desired surface chemistry, whether renal-clearable NPs will retain the EPR effect, a unique strength of conventional NPs in passive tumor targeting, is unknown but critical to their future applications in disease diagnosis and therapy. For the EPR effect to function well, NPs often need to remain in the blood plasma at a relatively high concentration for >6 h.[3b] Thus, macromolecules or NPs larger than 40 kDa or 5.5 nm that can escape kidney filtration generally exhibit the desired EPR effect.[3b,12a] However, to evade RES uptake, NPs must be smaller than the kidney filtration threshold (KFT) of 5.5 nm.[12a] These seemingly contradictory requirements on NP size naturally raise a fundamental question of whether renal-clearable NPs with HDs smaller than the KFT can still have prolonged retention times in tumors like their larger counterparts. In addition, since the imaging contrast index (CI), which reports the quality of imaging detection, is dependent on the ratio of the amount of probe in the tumor to that in the normal tissue background, clearance of the probes from normal tissues also plays a key role in contrast enhancement and rapid detection.[14] However, the way that renal-clearable NPs are eliminated from normal tissues in comparison with renal-clearable small molecules has not been investigated previously.

With these two fundamental questions, we conducted a detailed comparison of passive tumor targeting by renal-clearable near-IR (NIR)-emitting inorganic GS-AuNPs and a renal-clearable organic fluorophore, IRDye 800CW[15] (Figure 1). The synthesis of the 2.5 nm NIR-emitting GS-AuNPs was reported previously;[13b,16] the modified synthetic procedures are described in the Supporting Information (SI), and characterization data are shown in Figures S1−S3 in the SI. These two probes have comparable emission wavelengths (~800 nm) and high physiological and photostability suitable for real-time imaging of passive tumor targeting and retention kinetics in

Received: February 15, 2013
Published: March 19, 2013

dx.doi.org/10.1021/ja401612x | J. Am. Chem. Soc. 2013, 135, 4978−4981

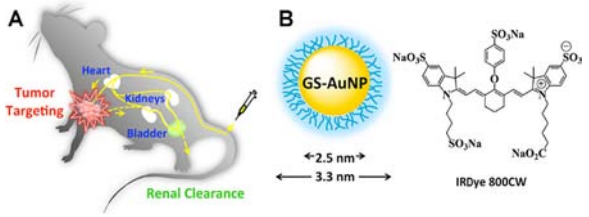

Figure 1. (A) Scheme of passive tumor targeting of renal-clearable probes. In vivo tumor targeting and clearance kinetics can be measured by fluorescence imaging in real time after iv injection of the probes into nude mice. (B) Schematic representation of a GS-AuNP (2.5 nm core size, HD = 3.3 nm) and the structure of IRDye 800CW.

tumor and normal tissues (Figure S4). While GS-AuNPs and IRDye 800CW behave similarly in initial tumor targeting, they exhibited distinct retention kinetics in tumor and normal tissues: GS-AuNPs were retained in the tumor at a concentration 10 times higher than the dye molecules 12 h p.i. but cleared from normal tissue >3 times faster than the dye molecules. As a result, the NPs reached the detection threshold (CI = 2.5) nearly 3 times faster than the dye molecules. These results clearly show that renal-clearable GS-AuNPs with HDs of 3.3 nm (smaller than the KFT of 5.5 nm) can passively target tumors through the EPR effect and are more suitable for rapid tumor detection than organic dye molecules. These new findings on passive tumor targeting by renal-clearable AuNPs, as distinct from small dye molecules and conventional non-renal-clearable NPs, will provide further guidance to chemists in designing a new generation of nanomedicines for clinical use.

Passive tumor targeting by GS-AuNPs and IRDye 800CW was investigated by collecting in situ fluorescence images of MCF-7 tumor-bearing nude mice at different p.i. time points (Figure 2A). While the mice were barely imaged in the NIR before injection of the probes, they became visible right after intravenous (iv) injection of the probes as a result of rapid distribution of the probes in the mice. However, tumor areas

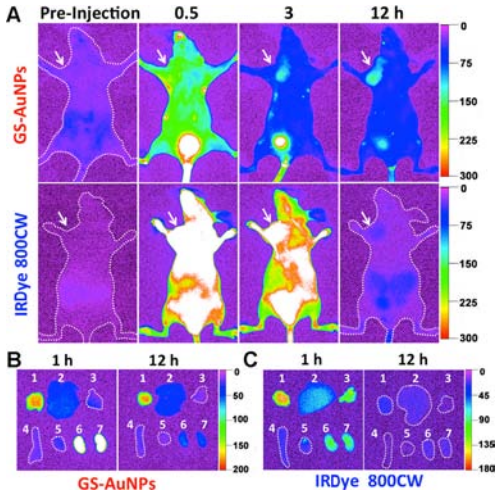

Figure 2. (A) Representative in vivo NIR fluorescence images of MCF-7 tumor-bearing mice iv-injected with GS-AuNPs and IRDye 800CW collected 0.5, 3, and 12 h p.i. The tumor areas are indicated with arrows. (B, C) Ex vivo fluorescence images of organs and tumors removed 1 and 12 h p.i. from MCF-7 tumor-bearing mice iv-injected with (B) GS-AuNPs and (C) IRDye 800CW. Labels: 1, tumor; 2, liver; 3, lung; 4, spleen; 5, heart; 6, kidney (left); 7, kidney (right). More images related to the tumor targeting by IRDye 800CW are shown in Figure S5.

were hardly defined in the mice in the first 0.5 h p.i. because of the strong fluorescence background from the probes in normal tissue (Figure 2A). With increasing time, the decrease in the fluorescence background from normal tissue caused the tumor areas to become readily defined in the mouse injected with GS-AuNPs at 3 h p.i. (Figure 2A), whereas for the mouse injected with dye molecules, an additional 5 h was required to obtain clear tumor images (Figure S5). At 12 h p.i., the tumor area in the mouse injected with GS-AuNPs was more evident because of the well-maintained signal from the tumor site and the further decrease in the fluorescence background from normal tissue. In contrast, the significant decrease in emission from the tumor in the dye-injected mouse indicated that most of the dye molecules had been eliminated from the tumor 12 h p.i. (Figures 2A and S5). Besides the tumor, the bladder was another place where the accumulation and elimination of both probes were readily observed (Figure 2A). This confirmed the renal clearance of the NPs and the dye, consistent with the previous observations of luminescent GS-AuNPs[13b,c] and IRDye 800CW.[15]

Ex vivo images of organs and tumors taken from the probe-injected mice showed that the tumors taken at 1 and 12 h p.i. from the mice injected with GS-AuNPs exhibited comparable signals (Figure 2B), while the signal from the tumor taken from the dye-injected mouse at 12 h p.i. was significantly lower than the one taken at 1 h p.i. (Figure 2C), further confirming the much longer tumor retention time of GS-AuNPs. However, for both probes, the signals in the kidney were significantly lower at 12 h p.i. than at 1 h p.i. (Figure 2B,C), indicating that both probes were cleared from the body through kidney filtration. The consistency in the accumulation of the probes in the tumor and kidney from the in vivo and ex vivo studies clearly indicates that noninvasive real-time in vivo imaging of tumor targeting and renal clearance of these probes is feasible.

As the CI is a general parameter used in tumor imaging to evaluate how well the tumor can be distinguished from normal tissue as a result of the introduction of a probe,[17] we quantified the time-dependent CI values for GS-AuNPs and IRDye 800CW. Generally, a CI value of 2.5 is considered to be the threshold for substantial tumor targeting.[18] The NPs and dye molecules took 3.1 ± 0.2 and 8.2 ± 0.6 h, respectively, to reach a CI value of 2.5 (Figures 3A and S6 and Table S1). While the CI value of ∼3.0 for GS-AuNPs is slightly lower than that for the reported renal-clearable QDs conjugated with active tumor-targeting ligands (5.0), it is higher than that for renal-clearable QDs without active targeting ligands (1.8).[12b] The differences in the CI kinetics for the NPs and the dye fundamentally arise from the distinctive retention kinetics of the two probes in normal tissue and tumors. As shown in Figures 3B and S7, the fluorescence intensity of normal tissue in the mice injected with IRDye 800CW reached its maximum 40−50 min p.i., but that of mice injected with GS-AuNPs took <10 min to reach its maximum (Figure 3B and Table S2). The retention kinetics of IRDye 800CW in normal tissue exhibited a monoexponential decay with a half-life of 2.3 ± 0.3 h (Figure 3B). In contrast, GS-AuNPs in normal tissue showed a two-compartment decay: >90% of the NPs were eliminated from the normal tissue with a half-life of 43.4 ± 6.6 min, and <10% of the NPs remained in the normal tissue for >24 h. These results indicate that most of the NPs were cleared from the normal tissue >3 times faster than the dye molecules.

Subsequent analysis of the time-dependent emission intensities from the tumors also revealed some similarities and differences in the tumor targeting by the NPs and dye molecules (Figures 3C and S8). Both probes reached their maximum

dx.doi.org/10.1021/ja401612x | J. Am. Chem. Soc. 2013, 135, 4978−4981

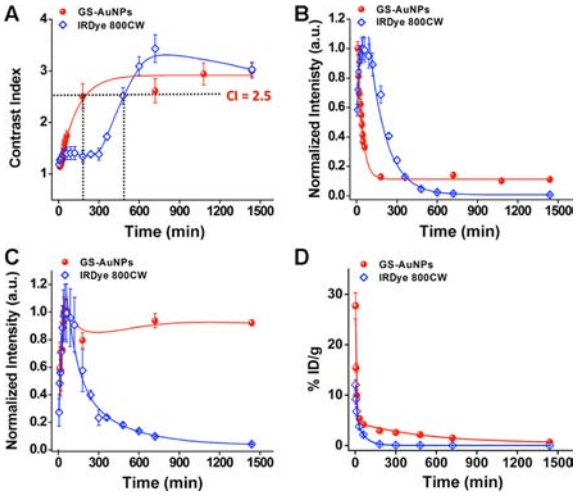

Figure 3. (A) Contrast index (CI) of GS-AuNPs and IRDye 800CW at different p.i. time points. The NPs reached the maximum CI value faster than the dye. The CI threshold value of 2.5 was reached in 3.1 ± 0.2 and 8.2 ± 0.6 h for the NPs and the dye, respectively. (B) Retention kinetics in normal tissue. The retention half-lives of GS-AuNPs and IRDye 800CW are 43.4 ± 6.6 min and 2.3 ± 0.3 h, respectively (n = 3). (C) Tumor targeting kinetics of GS-AuNPs and IRDye 800CW, respectively. (D) Pharmacokinetics of the renal-clearable GS-AuNPs and IRDye 800CW 0−24 h p.i. The curves were fitted to biexponential function with R^2 values of 0.9711 and 0.9838, respectively. The distribution half-lives ($t_{1/2\alpha}$) are 5.4 ± 1.2 and 6.3 ± 2.5 min, respectively, and the elimination half-lives ($t_{1/2\beta}$) are 8.5 ± 2.1 and 0.98 ± 0.08 h, respectively (means ± standard deviations, n = 3).

accumulations at the tumor sites within 40 min, indicating that the NPs behaved like the small dye molecules in the initial stage of the tumor targeting. However, the retention kinetics of the NPs and dye molecules in the tumor were different. IRDye 800CW followed a biexponential decay with half-lives of 1.4 ± 0.6 h (70.7 ± 9.2%) and 6.2 ± 0.3 h (29.3 ± 9.2%). While the origin of this two-compartment decay is still not clear, we hypothesize that the observed shorter half-life (~1.4 h) might result from the dense blood vessels in tumors, making the dye molecules diffuse away from the tumors more easily than from normal tissue (2.3 ± 0.3 h). However, the longer half-life (6.2 ± 0.3 h) might be due to the leakiness of the tumor vascular structure and trapping of the dye molecules inside the tumor. Less than 5% of the maximum fluorescence intensity remained in the tumor site 24 h p.i., indicating that the dye molecules can be eventually cleared from the tumors. In sharp contrast, >76% of the maximum fluorescence intensity from the NPs remained in the tumor 24 h p.i., which implies that the tumor retention of GS-AuNPs is much longer than that of IRDye 800CW. Such distinct tumor retention behavior for GS-AuNPs and IRDye 800 CW suggests that the EPR effect does exist for GS-AuNPs even though their HD of 3.3 nm is smaller than KFT of 5.5 nm.

We then compared the pharmacokinetics of GS-AuNPs and IRDye 800CW in nude mice to obtain a better understanding of the origin of the EPR effect. While the NPs and dye are both renal-clearable, their pharmacokinetics are not exactly the same. Both GS-AuNPs and IRDye 800CW followed two-compartment pharmacokinetics with comparable distribution half-lives ($t_{1/2\alpha}$) of 5.4 ± 1.2 and 6.3 ± 2.5 min, respectively (Figure 3D). The very short $t_{1/2\alpha}$ is typical of many small molecular probes (e.g., $t_{1/2\alpha}$ = 0.4 min for Gd-DTPA[6] and 16.2 min for iomeprol[7]). Since $t_{1/2\alpha}$ reflects how fast a probe is distributed in the body, the very short $t_{1/2\alpha}$ for the renal-clearable GS-AuNPs indicates that they behave more like small molecules than conventional large NPs in their initial tissue distribution,[13b] consistent with their initial tumor targeting. However, the blood-elimination half-life ($t_{1/2\beta}$) for the GS-AuNPs in nude mice was 8.5 ± 2.1 h, which is slightly shorter than the $t_{1/2\beta}$ observed in balb/c mice (12.7 h)[13b] but nearly 9 times longer than that of the dye (0.98 ± 0.08 h). Such a long $t_{1/2\beta}$ is the origin of the EPR effect in renal-clearable GS-AuNPs, as it exceeds the minimum requirement of 6 h for a strong EPR effect.[3b] The $t_{1/2\beta}$ of GS-AuNPs (8.5 h) is 4 times longer than that of 5.5 nm renal-clearable cysteine-coated (~2 h),[12] which also explains why the CI of GS-AuNPs (~3.0) is higher than that of renal-clearable QDs without active targeting ligands (1.8).[12b]

To gain a more quantitative understanding of the in vivo behaviors of the two probes, we studied the biodistribution of the NPs and dye molecules at 1 and 12 h (Figure 4A,B). The tumor

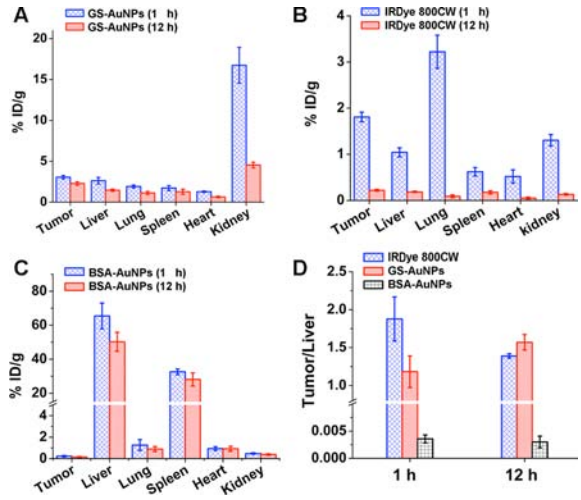

Figure 4. (A−C) Biodistributions of (A) GS-AuNPs, (B) IRDye 800CW, and (C) BSA-AuNPs at 1 and 12 h p.i. (D) Ratios of the probe concentration in tumor to that in liver at 1 and 12 h p.i..

uptakes were measured to be 3.0 ± 0.2 and 2.3 ± 0.2% ID/g for the GS-AuNPs and 1.8 ± 0.1 and 0.2 ± 0.02% ID/g for IRDye 800 CW at 1 and 12 h, respectively, demonstrating that GS-AuNPs are retained in the tumor much longer than IRDye 800CW and at a concentration 10 times higher than that of the dye molecules at 12 h p.i., consistent with the in vivo kinetics results (Figures 2 and 3A−C). This prolonged tumor retention behavior is very similar to that reported for large PEG-coated AuNPs (PEG-AuNPs) with sizes of 20−100 nm, which also exhibit long tumor retention times due to the EPR effect.[19] The reason that the EPR effect is observed for GS-AuNPs is because GSH behaves like the PEG molecule in resisting serum protein adsorption, which allows the GS-AuNPs, like those 20−100 nm PEG-AuNPs,[19] to be retained in the blood plasma at a relatively high concentration in tumor targeting. However, it should be noted that GS-AuNPs do exhibit some differences in some passive tumor targeting behaviors compared with those non-renal-clearable PEG-AuNPs.[19] In terms of tumor accumulation kinetics, GS-AuNPs reached their highest accumulation within 1 h; this is much faster than for the large PEG-AuNPs,[19] which generally reach their maxima 4−8 h p.i.. Also, the targeting efficacy of GS-AuNPs is generally 2−10 times better than those of 20−100 nm PEG-AuNPs.[19] Another advantage of renal-clearable AuNPs over non-renal-clearable ones is that the targeting specificity of the GS-AuNPs is much higher. As a

dx.doi.org/10.1021/ja401612x | J. Am. Chem. Soc. 2013, 135, 4978−4981

control, we investigated the tumor targeting specificity of ~30 nm bovine serum albumin (BSA)-coated AuNPs (BSA-AuNPs) (HD ≈ 60 nm; Figure S10) under the same conditions and found that >70% ID were rapidly shuttled out of circulation to the liver and spleen (Figure 4C). As a result, the tumor targeting specificities of 30 nm BSA-AuNPs were only 0.0036 ± 0.0007 and 0.0030 ± 0.001 at 1 and 12 h, respectively, which are >300 times less than those of GS-AuNPs and the dye (Figure 4D). Generally, the targeting specificity of GS-AuNPs is one or two orders of magnitude better than those of non-renal-clearable AuNPs because accumulation of GS-AuNPs in the RES is >10 times lower than those of large AuNPs (30−60% ID/g).[4,19,20]

In summary, we have systematically compared in vivo passive tumor targeting by renal-clearable GS-AuNPs and IRDye 800CW. While the NPs behave like the small dye molecules in the initial stage of tumor targeting, the tumor retention time of the NPs is much longer than that of the dye molecules, indicating that GS-AuNPs do retain the EPR effect while achieving efficient renal clearance. The EPR effect for the GS-AuNPs likely occurs because GS-AuNPs evade uptake by the RES organs and are retained in the blood plasma with a relatively long elimination half-life of 8.5 h. In addition, clearance of GS-AuNPs from normal tissues is >3 times faster than that of the dye molecules. Thus, the CI of the NPs increases more rapidly than that of the small dye molecules (3 h vs 8 h), implying that the GS-AuNPs are more suitable for rapid detection of tumors than IRDye 800CW. With rapid clearance in normal tissue, long retention in tumors, and high tumor targeting specificity, these renal-clearable luminescent AuNPs circumvent the dilemma of different size requirements for the EPR effect and minimization of RES uptake and thus hold great promise for the application of inorganic nanomedicines in clinical practice.

■ ASSOCIATED CONTENT

Supporting Information

Experimental methods and additional data. This material is available free of charge via the Internet at http://pubs.acs.org.

■ AUTHOR INFORMATION

Corresponding Author

jiezheng@utdallas.edu

Notes

The authors declare no competing financial interest.

■ ACKNOWLEDGMENTS

This work was supported in part by the NIH (R21EB009853 and 1R21EB011762), CPRIT (RP120588), and the startup fund of the UT Dallas (J.Z.). We thank Dr. Li Liu at UT Southwestern Medical Center for teaching tumor implantation.

■ REFERENCES

(1) (a) Qian, H.; Eckenhoff, W. T.; Zhu, Y.; Pintauer, T.; Jin, R. *J. Am. Chem. Soc.* **2010**, *132*, 8280. (b) Liu, Y. D.; Han, X. G.; He, L.; Yin, Y. D. *Angew. Chem., Int. Ed.* **2012**, *51*, 6373. (c) Zrazhevskiy, P.; Sena, M.; Gao, X. H. *Chem. Soc. Rev.* **2010**, *39*, 4326.

(2) (a) Ferrari, M. *Nat. Rev. Cancer* **2005**, *5*, 161. (b) Huang, X. H.; Peng, X. H.; Wang, Y. Q.; Wang, Y. X.; Shin, D. M.; El-Sayed, M. A.; Nie, S. M. *ACS Nano* **2010**, *4*, 5887. (c) Xing, H.; Wong, N. Y.; Xiang, Y.; Lu, Y. *Curr. Opin. Chem. Biol.* **2012**, *16*, 429. (d) Zhou, M.; Zhang, R.; Huang, M.; Lu, W.; Song, S.; Melancon, M. P.; Tian, M.; Liang, D.; Li, C. *J. Am. Chem. Soc.* **2010**, *132*, 15351. (e) Cheng, Y.; Samia, A. C.; Meyers, J. D.; Panagopoulos, I.; Fei, B.; Burda, C. *J. Am. Chem. Soc.* **2008**, *130*, 10643. (f) Chou, S. W.; Shau, Y. H.; Wu, P. C.; Yang, Y. S.; Shieh, D. B.; Chen, C. C. *J. Am. Chem. Soc.* **2010**, *132*, 13270. (g) Lee, H.; Yu, M. K.; Park, S.; Moon, S.; Min, J. J.; Jeong, Y. Y.; Kang, H. W.; Jon, S. *J. Am. Chem. Soc.* **2007**, *129*, 12739. (h) Robinson, J. T.; Hong, G.; Liang, Y.; Zhang, B.; Yaghi, O. K.; Dai, H. *J. Am. Chem. Soc.* **2012**, *134*, 10664. (i) Lee, J. E.; Lee, N.; Kim, H.; Kim, J.; Choi, S. H.; Kim, J. H.; Kim, T.; Song, I. C.; Park, S. P.; Moon, W. K.; Hyeon, T. *J. Am. Chem. Soc.* **2010**, *132*, 552. (j) Ling, D.; Park, W.; Park, Y. I.; Lee, N.; Li, F.; Song, C.; Yang, S. G.; Choi, S. H.; Na, K.; Hyeon, T. *Angew. Chem., Int. Ed.* **2011**, *50*, 11360.

(3) (a) Matsumura, Y.; Maeda, H. *Cancer Res.* **1986**, *46*, 6387. (b) Iyer, A. K.; Khaled, G.; Fang, J.; Maeda, H. *Drug Discovery Today* **2006**, *11*, 812.

(4) Wang, Y.; Liu, Y.; Luehmann, H.; Xia, X.; Brown, P.; Jarreau, C.; Welch, M.; Xia, Y. *ACS Nano* **2012**, *6*, 5880.

(5) Liu, R. S.; Chou, T. K.; Chang, C. H.; Wu, C. Y.; Chang, C. W.; Chang, T. J.; Wang, S. J.; Lin, W. J.; Wang, H. E. *Nucl. Med. Biol.* **2009**, *36*, 305.

(6) Kobayashi, H.; Sato, N.; Hiraga, A.; Saga, T.; Nakamoto, Y.; Ueda, H.; Konishi, J.; Togashi, K.; Brechbiel, M. W. *Magn. Reson. Med.* **2001**, *45*, 454.

(7) Lorusso, V.; Taroni, P.; Alvino, S.; Spinazzi, A. *Invest. Radiol.* **2001**, *36*, 309.

(8) Zamboni, W. C. *Clin. Cancer Res.* **2005**, *11*, 8230.

(9) (a) Dobrovolskaia, M. A.; McNeil, S. E. *Nat. Nanotechnol.* **2007**, *2*, 469. (b) Kareem, H.; Sandstrom, K.; Elia, R.; Gedda, L.; Anniko, M.; Lundqvist, H.; Nestor, M. *Tumor Biol.* **2010**, *31*, 79.

(10) Yang, R. H.; Chang, L. W.; Wu, J. P.; Tsai, M. H.; Wang, H. J.; Kuo, Y. C.; Yeh, T. K.; Yang, C. S.; Lin, P. *Environ. Health Persp.* **2007**, *115*, 1339.

(11) (a) Park, J. H.; Gu, L.; von Maltzahn, G.; Ruoslahti, E.; Bhatia, S. N.; Sailor, M. J. *Nat. Mater.* **2009**, *8*, 331. (b) Choi, H. S.; Ipe, B. I.; Misra, P.; Lee, J. H.; Bawendi, M. G.; Frangioni, J. V. *Nano Lett.* **2009**, *9*, 2354. (c) Gao, J.; Chen, K.; Xie, R.; Xie, J.; Lee, S.; Cheng, Z.; Peng, X.; Chen, X. *Small* **2010**, *6*, 256. (d) Lux, F.; Mignot, A.; Mowat, P.; Louis, C.; Dufort, S.; Bernhard, C.; Denat, F.; Boschetti, F.; Brunet, C.; Antoine, R.; Dugourd, P.; Laurent, S.; Vander Elst, L.; Muller, R.; Sancey, L.; Josserand, V.; Coll, J. L.; Stupar, V.; Barbier, E.; Remy, C.; Broisat, A.; Ghezzi, C.; Le Duc, G.; Roux, S.; Perriat, P.; Tillement, O. *Angew. Chem., Int. Ed.* **2011**, *50*, 12299.

(12) (a) Choi, H. S.; Liu, W.; Misra, P.; Tanaka, E.; Zimmer, J. P.; Ipe, B. I.; Bawendi, M. G.; Frangioni, J. V. *Nat. Biotechnol.* **2007**, *25*, 1165. (b) Choi, H. S.; Liu, W. H.; Liu, F. B.; Nasr, K.; Misra, P.; Bawendi, M. G.; Frangioni, J. V. *Nat. Nanotechnol.* **2010**, *5*, 42.

(13) (a) Yu, M. X.; Zhou, C.; Liu, J. B.; Hankins, J. D.; Zheng, J. *J. Am. Chem. Soc.* **2011**, *133*, 11014. (b) Zhou, C.; Hao, G. Y.; Thomas, P.; Liu, J. B.; Yu, M. X.; Sun, S. S.; Oz, O. K.; Sun, X. K.; Zheng, J. *Angew. Chem., Int. Ed.* **2012**, *51*, 10118. (c) Zhou, C.; Long, M.; Qin, Y.; Sun, X.; Zheng, J. *Angew. Chem., Int. Ed.* **2011**, *50*, 3168. (d) Zhou, C.; Sun, C.; Yu, M. X.; Qin, Y. P.; Wang, J. G.; Kim, M.; Zheng, J. *J. Phys. Chem. C* **2010**, *114*, 7727. (e) Zheng, J.; Zhou, C.; Yu, M. Y.; Liu, J. B. *Nanoscale* **2012**, *4*, 4073.

(14) Kobayashi, H.; Longmire, M. R.; Ogawa, M.; Choyke, P. L. *Chem. Soc. Rev.* **2011**, *40*, 4626.

(15) Marshall, M. V.; Draney, D.; Sevick-Muraca, E. M.; Olive, D. M. *Mol. Imaging Biol.* **2010**, *12*, 583.

(16) Tu, X.; Chen, W.; Guo, X. *Nanotechnology* **2011**, *22*, No. 095701.

(17) Jiang, T.; Olson, E. S.; Nguyen, Q. T.; Roy, M.; Jennings, P. A.; Tsien, R. Y. *Proc. Natl. Acad. Sci. U.S.A.* **2004**, *101*, 17867.

(18) (a) Andreev, O. A.; Dupuy, A. D.; Segala, M.; Sandugu, S.; Serra, D. A.; Chichester, C. O.; Engelman, D. M.; Reshetnyak, Y. K. *Proc. Natl. Acad. Sci. U.S.A.* **2007**, *104*, 7893. (b) Zhang, E. L.; Zhang, C.; Su, Y. P.; Cheng, T. M.; Shi, C. M. *Drug Discovery Today* **2011**, *16*, 140.

(19) Perrault, S. D.; Walkey, C.; Jennings, T.; Fischer, H. C.; Chan, W. C. W. *Nano Lett.* **2009**, *9*, 1909.

(20) (a) Puvanakrishnan, P.; Park, J.; Chatterjee, D.; Krishnan, S.; Tunnell, J. W. *Int. J. Nanomed.* **2012**, *7*, 1251. (b) Zhang, G.; Yang, Z.; Lu, W.; Zhang, R.; Huang, Q.; Tian, M.; Li, L.; Liang, D.; Li, C. *Biomaterials* **2009**, *30*, 1928.